J. Fluid Mech. (1993), *vol.* 249, *pp.* 307–336

Resonance in axisymmetric jets with controlled helical-mode input

By T. C. CORKE AND S. M. KUSEK

Illinois Institute of Technology, Fluid Dynamics Research Center, Mechanical and Aerospace Engineering Department, Chicago, IL 60616, USA

(Received 8 April 1992 and in revised form 16 October 1992)

This work involves active control of fundamental two- and three-dimensional amplified modes in an axisymmetric jet by introducing localized acoustic disturbances produced by an azimuthal array of miniature speakers placed close to the jet lip on the exit face. The independent control of each speaker output allowed different azimuthal amplitude and phase distributions of periodic inputs. The types of inputs used in this study consisted of conditions to force helical mode pairs with the same frequency and equal but opposite azimuthal wavenumbers, $m = \pm 1$, separately, or with axisymmetric ($m = 0$) modes. Three forcing conditions were studied in detail. The first consisted of a weakly amplified helical mode pair which was essentially 'superposed' with the natural jet instability modes. This provided a reference to the second case which consisted of the same helical mode pairs along with an axisymmetric mode at the harmonic streamwise wavenumber. This combination led to the resonant growth of the otherwise weakly (linear) amplified subharmonic helical modes. A weakly nonlinear three-wave amplitude evolution equation with a coupling coefficient derived from the data was found to model the enhanced growth of the subharmonic helical modes well. The third case consisted of forcing only $m = \pm 1$ helical modes at a frequency which was close to the most amplified. This was compared to the results of Corke *et al.* (1991) who forced an axisymmetric mode at the same frequency and found it to lead to the enhanced growth of near-subharmonic modes, as well as numerous sum and difference modes. The helical modes had effects identical to the previous work and confirmed the resonant amplification of a near-subharmonic mode. The amplitude development was also well represented by the nonlinear amplitude equation, including the dependence of the streamwise amplification rate on the azimuthal change in the fundamental-mode initial amplitude. However, the coupling coefficient in this case was approximately one-third that with exact fundamental–subharmonic resonance. Finally we offer some explanation for the selection of the different mode frequencies in this case.

1. Introduction

During the past few decades, many theoretical and experimental studies have been done to enhance our understanding of the evolution of the flow in axisymmetric jets. From these many investigations, some observations are universally apparent. Among these is the complication (and added interest) of studying this flow, which stems from the fact that the axisymmetric jet has two distinct lengthscales, the momentum thickness, θ, and the jet diameter, D. The momentum thickness is generally the appropriate lengthscale for the near-field dynamics (near the jet exit), and the jet diameter generally governs the evolution in the far field (greater than

three diameters downstream of the jet exit). Added to this, when the ratio of these two lengthscales (θ/D) is small, the initial shear-layer dynamics behave essentially as a plane mixing layer. Ultimately however, three-dimensional effects become more pronounced downstream as the initial shear layer spreads.

Linear stability analysis of axisymmetric jets with thin initial shear layers (i.e. $\theta/D \ll 1$), such as by Michalke (1971), Mattingly & Chang (1974) and Plaschko (1979), has predicted that the initial region of the jet is equally unstable to both axisymmetric ($m = 0$) and the first helical modes ($m = +$ or -1). This has been confirmed in the experiments of Drubka (1981), Strange & Crighton (1981), Cohen & Wygnanski (1987*a*, *b*), Rice, Raman & Reshotko (1990), Raman (1991) and Corke, Shakib & Nagib (1991). However, the short-time spectral estimates by Corke *et al.* (1991) indicated that these modes rarely (if ever) exist together. Rather, they were observed to non-deterministically switch from one mode type to the other, presumably as a result of stochastic disturbances at the jet exit lip.

Although the linear characteristics of these two modes are similar, Mankbadi & Liu (1981) have shown that their nonlinear development is quite different. As a result of nonlinear effects, the streamwise lifespan of the first helical mode is less than that of the axisymmetric mode. However, the mechanism which limits the streamwise extent of this mode also makes it more efficient in pumping energy into fine-scale incoherent motions. The net result is that helical modes are still more effective in enhancing fine-scale turbulence than their axisymmetric counterpart. Strange (1981) had observed this trend in his experiment where turbulent fluctuations were observed to increase significantly when the jet was excited with helical modes.

Since the streamwise extent of growth of a mode is proportional to its wavelength (energy saturation occurs after approximately four wavelengths downstream), longer-wavelength helical modes have a greater potential for a significant and sustaining influence on turbulence production in jets. From linear theory, such lower-frequency modes are considered less important owing to their lower amplification rates. However, in the presence of a properly selected more-amplified mode, intermodal energy transfer can lead to enhanced growth. A similar mechanism to this has been shown to govern the first development of three-dimensional modes in boundary layers (see for example Herbert 1988) and in wakes (Corke, Krull & Ghassemi 1992). In shear layers in jets, Cohen & Wygnanski (1987*a*, *b*) were the first to appreciate the significance of this mechanism. Although their analysis provides the framework for such interactions, the detailed measurements within the initial development region containing the linear and weakly nonlinear regimes was not complete. This work is an attempt to document this initial stage under conditions with controlled initial disturbances which promote the resonant growth of otherwise less-amplified helical modes in jets.

2. Experimental method

This experiment was performed in the same jet facility that was used by Drubka (1981), Shakib (1985), Corke *et al.* (1985, 1991), and Reisenthel, Xiong & Nagib (1991). Its very low core turbulence intensity level ($u'/U_j = 0.05\%$) makes it well suited for measurements on stability and mode interactions. The characteristics of this jet have been extensively documented in these cited investigations in terms of eigenmode distributions of the fundamental instability and of interacted modes, along with their dependence on changing initial conditions including Reynolds number, initial shear-layer thickness and core disturbance level.

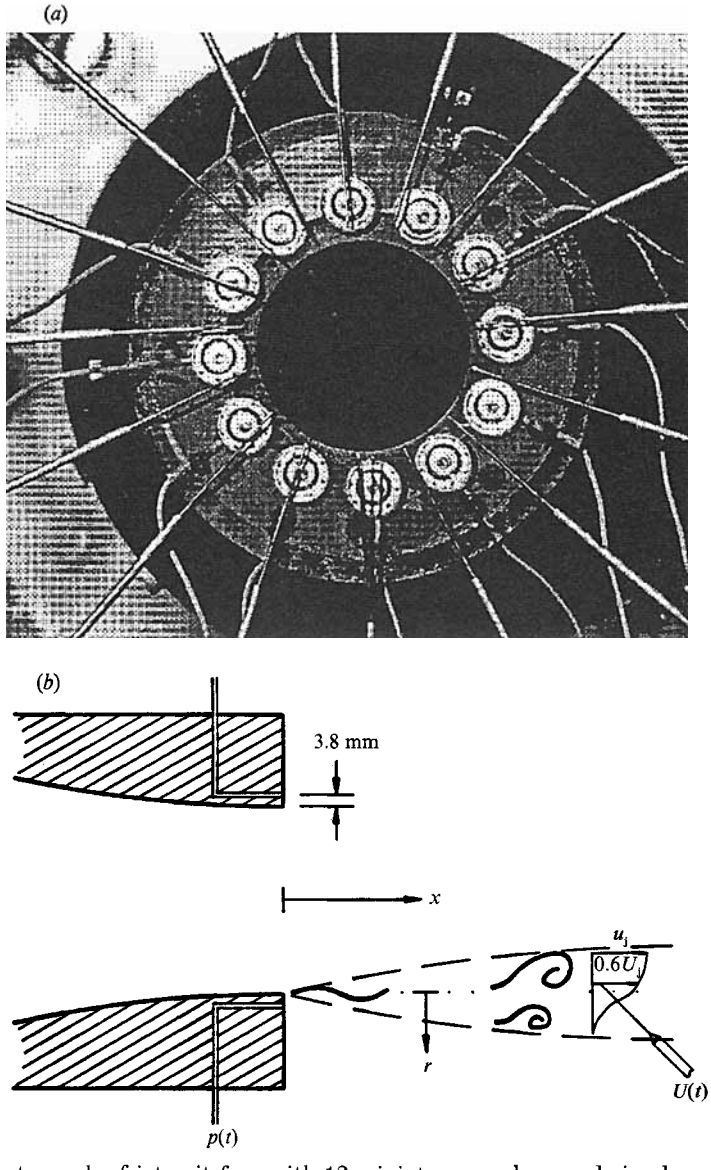

FIGURE 1. (a) Photograph of jet exit face with 12 miniature speakers and circular smoke-wire in place, and (*b*) schematic of coordinate system for measurements.

Our objective is to introduce disturbances at the lip of the jet that will promote the growth of axisymmetric and helical modes. In our previous work (Corke *et al.* 1991) we were only interested in forcing axisymmetric modes. In that case we could use a far-field sound source. In order to excite helical modes, we need an azimuthally varying amplitude distribution around the exit lip of the jet. To do this we placed an array of 12 miniature speakers on the exit face of the jet. Figure 1 (*a*) shows a photograph of the jet, viewed while looking upstream. The 12 speakers are visible as the small disks which rim the jet exit. To provide a scale, the jet exit diameter is 5.08 cm. Also seen in the photograph are the support arms (which appear as radial spokes) for a circular smoke-wire which was used for flow visualization.

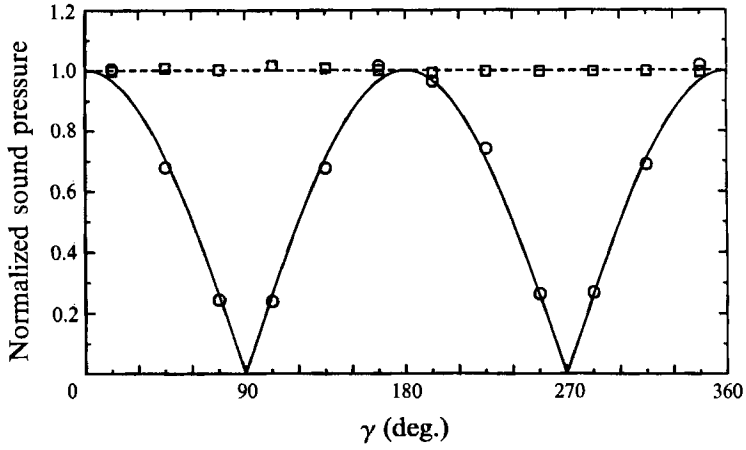

FIGURE 2. Azimuthal variation of normalized sound pressure amplitude from 12 speakers to seed $m = 0$ (□) and $m = \pm 1$ (○) modes.

Special care was taken in the design of the fixture for holding the speaker array. Specifically we were concerned with any passive influence that it would have on the basic flow. The basic flow and stability characteristics without and with the speaker array were documented by Kusek, Corke & Reisenthel (1990). These confirmed that it had a negligible passive influence on the flow.

For helical modes, our approach was to simultaneously introduce wave pairs with equal but opposite signed azimuthal wavenumbers. This is different from Cohen & Wygnanski (1987*b*) who introduced only a single helical mode. The motivation in our approach is that either signed mode has the same linear stability properties, and in an interaction with an axisymmetric mode with the harmonic streamwise wavenumber, the opposite signed helical mode will be produced. For example, the observation of a helical mode with the azimuthal wavenumber of the opposite sign to their forced helical mode was used by Cohen & Wygnanski to verify resonance. Long & Peterson (1922) introduced pairs of $m = \pm 1$ helical modes, without a simultaneous $m = 0$ mode.

To excite a helical mode with positive wavenumber m (clockwise moving), and frequency ω, the periodic time series to any individual speaker located at azimuthal angle γ would be $A_1(t,\gamma) = \mathscr{A} \sin(m\gamma + \omega t + \phi_1)$. Here, ϕ_1 is an arbitrary phase shift. The opposite-going, equal-amplitude helical mode with wavenumber $-m$ would be produced by the periodic function $A_2(t,\gamma) = \mathscr{A} \sin(-m\gamma + \omega t + \phi_2)$. The addition of these two periodic functions yields $A(t,\gamma) = 2\mathscr{A} \sin(\omega t + \frac{1}{2}(\phi_1 + \phi_2)) \cos(m\gamma + \frac{1}{2}(\phi_1 - \phi_2))$. Therefore, to produce equal and opposite helical modes with azimuthal wavenumber $\pm m$ and frequency ω, each speaker operates with a periodic input, $\sin(\omega t + \frac{1}{2}(\phi_1 + \phi_2))$, and amplitude determined by its azimuthal position according to $2\mathscr{A} \cos(m\gamma + \frac{1}{2}(\phi_1 - \phi_2))$. With 12 speakers it is possible to excite helical modes with azimuthal wavenumbers up to $m = \pm 6$, (i.e. every other speaker 180° apart in phase).

In this study we only introduced axisymmetric ($m = 0$) and $m = \pm 1$ helical modes. Figure 2 documents the measured sound pressure level from the speakers (symbols) and ideal amplitude (line) distributions in order to introduce these modes. In this case, it is presented as a rectified output, where a 180° phase shift actually occurs across the γ-locations of amplitude minima (90° and 270°).

Other than the method for introducing disturbances, the experimental conditions, and measurement and data processing techniques are similar to those previously used in this facility and reported by Corke *et al.* (1991). This experiment was performed at a single Reynolds number, $Re_D = 70000$, which was the upper value used in that previous work.

The measurements consisted of digitally acquiring voltage time series proportional to the unsteady pressure fluctuations at the exit lip of the jet and streamwise velocity component in the shear layer at different (x, r, γ)-locations. The coordinate frame is shown in the schematic of figure 1 (*b*). In the x-direction 11 equally spaced positions were sampled. These started just downstream of the jet exit lip and extended past the location of energy saturation of all the modes of interest. At any (x, γ)-location, 19 points were sampled in the radial direction. These were spaced to be at equal mean velocity increments, and extended from 0.99 to 0.1 U_j. To simulate traversing the velocity sensor in the γ-direction, the speaker array was rotated. This transformation is consistent for those modes which are introduced by the speaker array as well as those modes which are related to these through nonlinear interactions, as had earlier been confirmed with the use of a second hot-wire sensor. A total of seven azimuthal positions over a 180° span were sampled.

The velocity sensor and speaker array were moved by stepper motors under computer control. The accuracy in positioning the velocity sensor in the x- and r-directions was 10 and 5 μm respectively. The accuracy in the γ-direction for the speaker array was 0.5°.

The unsteady pressure at the lip of the jet was obtained from a B&K Type 2209 precision sound level meter which was connected to a pressure port through a short tubulation. The system amplitude response was flat to 4 kHz. As with Corke *et al.* (1991), only a single pressure port was used. This was located at the same physical azimuthal position as the velocity sensor.

The velocity sensor was a single hot wire operating in constant-temperature mode. The probe body was the same as that of Corke *et al.* (1991), which was designed to minimize any upstream influence caused by probe feedback.

The voltage time series from the sound level meter and constant-temperature anemometer were d.c. biased as necessary and amplified through an analog programmable gain circuit to minimize quantization error prior to being acquired by a digital computer. Also acquired for reference was the voltage series used to drive one of the speakers. The digital sampling rate was 16250 Hz. This allowed us to resolve frequencies up to three times that of the highest seeded mode. For each spatial sample, 32770 contiguous time samples were acquired for each of the three voltage inputs. This corresponded to 2.02 s of data or approximately 5000 cycles of the highest input frequency. Each of these formed a record of data. A total of 16 records for each spatial location were acquired.

Post processing consisted of digitally calibrating the pressure and velocity data series. For the velocity data, a fourth-order polynomial was used to linearize the anemometer output. Other processing generally involved calculating the mean and r.m.s. of the velocity fluctuations. Mode amplitudes and phase angles were determined from cross-spectral estimates using a 1024 point discrete Complex Fast Fourier Transform. Anti-alias filtering was done digitally prior to spectral calculations. To improve the convergence of the spectral estimates, a time-domain Hanning smoothing function was also used. The total of 512 record averages was found to be more than adequate to average out random variations in the spectra. The amplitudes corresponding to spectral peaks were converted to r.m.s. by taking the

Case	Re_D	f_f	m	$p'/q(\%)$	θ_i(mm)
A	70000	2500	0	0.016	0.095
		1250	± 1	0.037	
B	70000	1250	± 1	0.037	0.102
C	70000	2500	± 1	0.016	0.093

TABLE 1. Case study conditions

area under the peaks and normalizing them by the frequency bandwidth. For any mode, the local phase was the phase angle from the complex cross-spectra computed using velocity series at a given spatial location and the simultaneously sampled pressure at the jet lip. The streamwise spacing of data samples was close enough to guarantee at least two points within one wavelength of the modes of interest. This ensured that we could properly account for the 2π phase jumps which occur in the circular phase from one mode cycle to the next.

2.1. *Forcing conditions*

Given a fixed Reynolds number ($Re_D = 70000$), three initial disturbance conditions were examined. These are denoted as Cases A, B and C in table 1. Case B (the base case) consisted of introducing only helical mode pairs ($m = \pm 1$) at a frequency which was approximately one-half that of the most amplified initial mode (helical or axisymmetric). As such it is only weakly amplified. The initial amplitude of this mode was set to be low enough so that it would not interact or dominate over the other natural (stochastically forced) modes in the jet.

Case B was meant to be a reference for Case A in which we introduced, along with the helical mode pairs, an additional axisymmetric mode at the harmonic frequency of the helical mode. The choice of the axisymmetric mode frequency was expected to lead to the enhanced (resonant) growth of the subharmonic helical mode. The initial amplitude of the axisymmetric mode was set to be as low as possible but still be sufficient to lead to resonance.

In keeping with Corke *et al.* (1991), we defined the forcing amplitude in terms of the r.m.s. pressure fluctuations at the lip of the jet, p'. These values are shown in table 1 for the different cases, normalized by the dynamic pressure in the jet core, q. The unsteady pressure was measured using the sound level meter while connected to a pressure port without any flow through the jet. In the case of the helical mode it represents the maximum value.

Also compiled in table 1 are the values of the initial momentum thickness, θ_i, for the different cases. The initial value was estimated by linearly extrapolating the value at the lip from the measured values at the first three or four x-positions. As can be seen in figure 11 of Corke *et al.* (1991) (and figure 20 here), in the initial region up to approximately $x/D = 0.15$, the growth in the momentum thickness is slow and well approximated by a linear function. The deviation in the estimate of the initial momentum thickness is small among the cases here, indicating a relative lack of influence of the different forcing conditions. As such, we believe the differences between them is a measure of the uncertainty. Compared to the values of Corke *et al.* (1991), our θ_i are approximately 20% lower (this is also based on linear extrapolation to the lip of their values). We believe that this difference might be due to our not including mean profile values of less than $0.10/U_j$. The reason for excluding these was the general difficulty of getting stable averages at these lower velocities owing to the

high static sensitivity of constant-temperature hot wire on this regime. We believe that our current approach is more accurate for comparing the effect of forcing on the momentum thickness between cases at the same Reynolds number. However, we will continue to use the values (20% higher) of the momentum thickness from Corke *et al.* (1991) for defining the Strouhal numbers of the different modes.

Finally, the conditions of Case C are the counterpart to the forced case in Corke *et al.* (1991). The basic difference between them is that in our experiment the forced mode is $m = \pm 1$ helical wave pairs, compared to the $m = 0$ wave used in the previous work. The frequency of the forced modes is the same. In the previous work, forcing an $m = 0$ mode at this frequency led to numerous nonlinear sum and difference interactions (see for example figure 39 of Corke *et al.* 1991). It was intended that comparing the results with different initial mode types would help us to understand the origin of these interactions, which appear to be special in this case.

3. Results

As partial documentation of the basic flow, normalized mean velocity profiles at different x-positions for Case B are shown in figure 3. We believe that the selection of the forcing frequency in this case and low forcing amplitude leave the basic flow essentially unchanged compared to a natural (unforced) jet. To demonstrate this, we have included in figure 3(*a*), the mean profile from Drubka (1981) at a comparable Reynolds number ($Re_D = 62\,500$, $x/D = 0.17$) in the same jet. His was the case of a natural jet, without our added azimuthal speaker array at the nozzle exit. The comparison to the present data is very good. Within the linear growth region (for example up to $x/D = 0.2$ in Case B) the mean velocity profiles in figure 3 are representative of the three cases (A–C): all showed the same profile shape and degree of self-similarity. Beyond energy saturation, they also show a similar change in the mean profile, such as seen in figure 3(*b*).

3.1. *Thin-shear-layer assumption*

An important part of the recent studies by Cohen & Wygnanski (1987*a*) and Ahmadi-Moghadam (1986) was the quasi-two-dimensionality, from a linear stability standpoint, of the exit shear layer. Cohen & Wygnanski indicated that when the jet diameter is large compared to the shear-layer thickness, an increasing number of azimuthal modes become unstable. Their results specifically showed that for a ratio of the half-radius of the jet column to shear-layer momentum thickness ($r_{\frac{1}{2}}/\theta_i$) equal to 77, the amplification rates of modes with azimuthal wavenumbers from 1 to 6 were essentially indistinguishable. Their analysis was derived using a modified hyperbolic tangent mean profile with fitting coefficients determined from their experiment. A possibly more general result for a Blasius shear-layer profile by Ahmadi-Moghadam (1986) shows virtually no difference in amplification characteristics for azimuthal wavenumbers up to $m = 4$ for $r_{\frac{1}{2}}\theta_i = 100$.

Using an average value from table 1 for θ_i, for our jet $r_{\frac{1}{2}}/\theta_i = 263$. Therefore this jet far exceeds the criterion for a thin shear layer, and one should expect a close correspondence between the linear stability characteristics of the axisymmetric ($m = 0$) and $m = \pm 1$ helical modes, with the same frequency.

To test the validity of this assumption, the initial growth region of the forced axisymmetric mode in Case A and the forced helical mode in Case C were compared. Both these modes are at the same frequency. A general comparison can be made between the contours of constant eigenfunction modulus, given as $\log_{10} u'(f)/U_j$, for

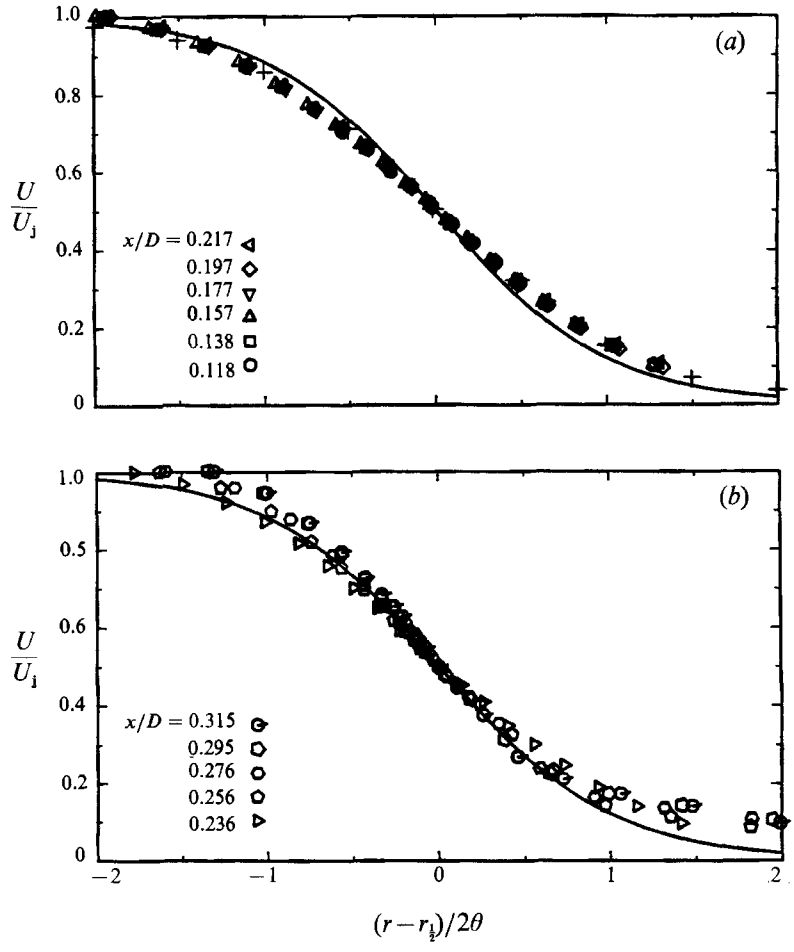

FIGURE 3. Mean velocity distribution across shear layer at different downstream locations in Case B, with comparison to hyperbolic tangent profile (——) and, in (*a*), natural (unforced) jet of Drubka (1981).

both modes in the (r, x)-plane seen in figure 4. In order to generate the contours, the values at discrete (r, x)-locations were first spline-fitted in both directions. A very low damping coefficient was used in order to not alter the actual data values. The constant-level contours were generated from these spline function fits. For the helical mode (figure 4*b*), the data are at the γ-position where the amplitude is a maximum. Even beyond the linear growth range ($x/D = 0.2$) the fluctuation distributions are very similar.

The eigenfunction modulus and phase distributions in the radial direction for these two modes are shown in figure 5, for different x-locations within the linear region. For the moduli, the values have been normalized by the radially integrated eigenfunction,

$$u_{\text{int}} = \frac{1}{\theta_1} \int_{r@u/U_j=0.10}^{r@u/U_j=0.99} u'(f)\, \mathrm{d}r.$$

Again, the eigenfunctions for the two modes are nearly identical. The streamwise development of normalized amplitude, u'_{int}/U_j, for the two modes is shown in figure

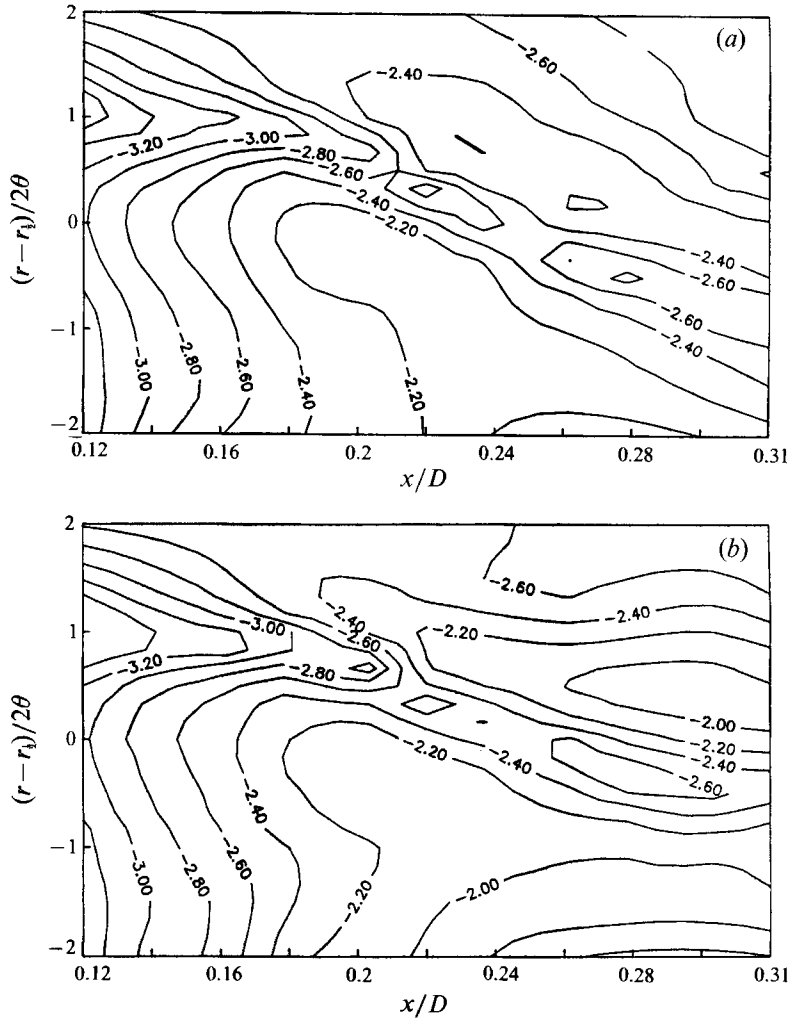

FIGURE 4. Contours of constant eigenfunction modulus for (*a*) Case A, $m = 0$, and (*b*) Case B, $m = \pm 1$ modes, both seeded at 2500 Hz. Levels correspond to $\log_{10}(u'/U_j)$.

6. In each case, the different symbols correspond to the amplitude growth at different azimuthal positions. For the $m = \pm 1$ mode of Case C, the initial amplitude varies with γ according to the forcing level distribution previously shown in figure 2. This accounts for the linear shift between growth curves at different γ-positions in that case. However, the amplification rate is independent of the γ-position.

A fit of the exponential growth of both modes in the two cases gave the same dimensionless amplification rate, $-\alpha_i \theta_i = 0.068$. The line drawn in figure 6 corresponds to that amplification rate. The linear theory prediction from Monkewitz & Huerre (1982) for a hyperbolic tangent mean profile is $-\alpha_i \theta_i = 0.073$. Our mean profiles fall between hyperbolic tangent and Blasius. For a Blasius profile, Ahmadi-Moghadam (1986) gives a value of 0.063.

A linear fit of the streamwise phase change in the x-direction gave values for the phase velocities of $C_r/U_j = 0.57$ for the $m = 0$ mode, and 0.53 for the $m = \pm 1$ mode. The difference between them is within the accuracy of our measurements and linear fit. The value from Monkewitz & Huerre is 0.63.

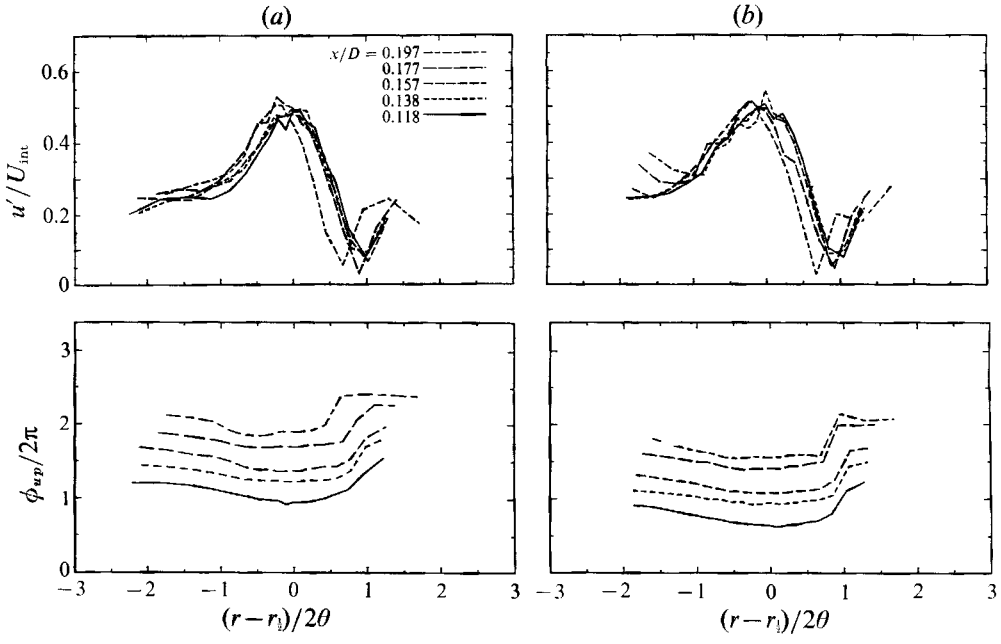

FIGURE 5. Eigenfunction modulus and phase in the r-direction for (a) Case A, $m = 0$ and (b) Case C, $m = \pm 1$ modes, both seeded at 2500 Hz.

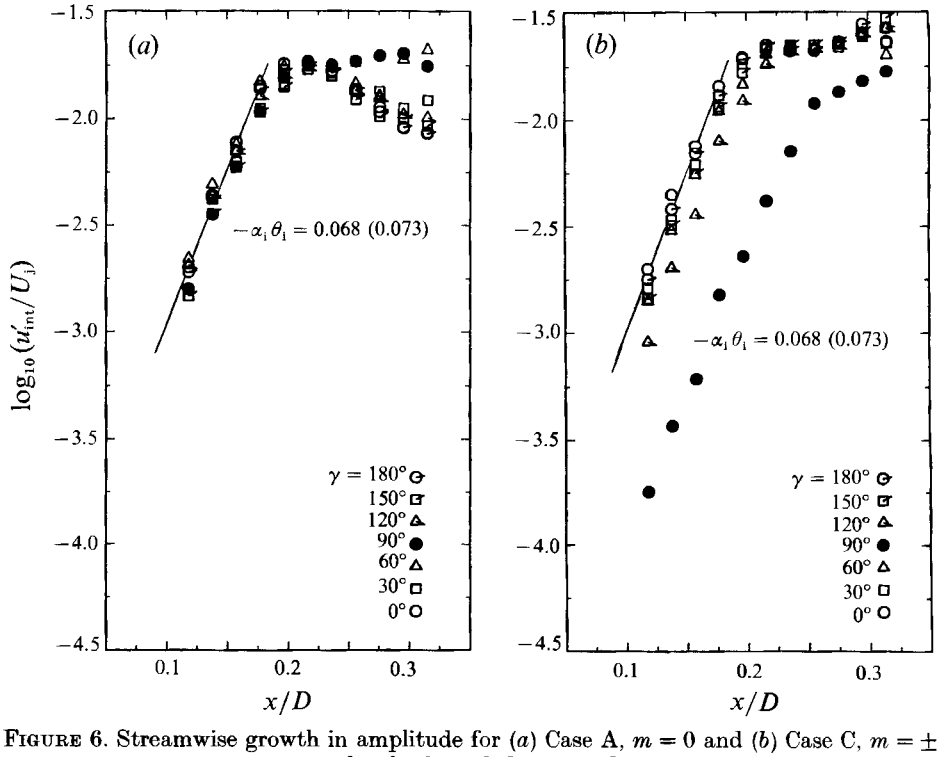

FIGURE 6. Streamwise growth in amplitude for (a) Case A, $m = 0$ and (b) Case C, $m = \pm 1$ modes, both seeded at 2500 Hz.

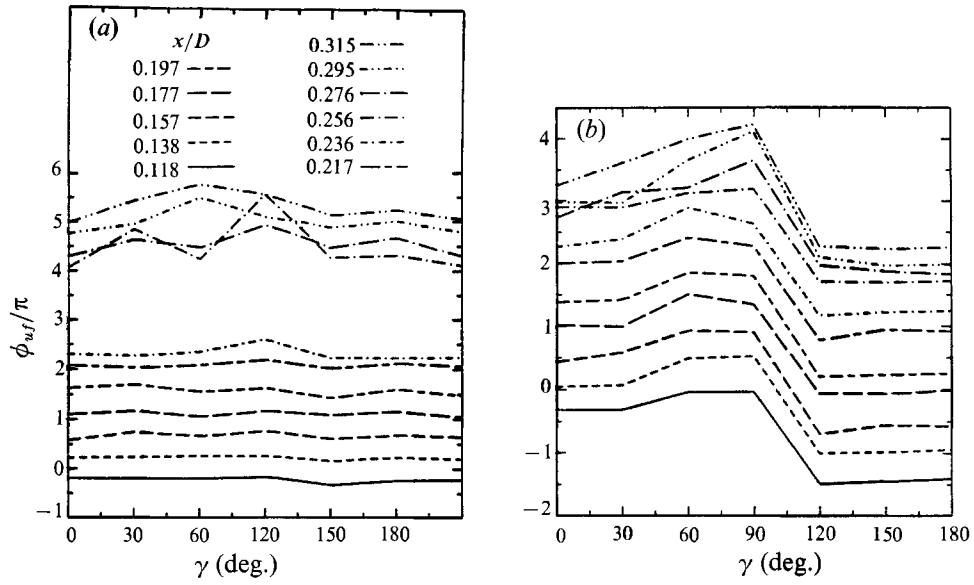

FIGURE 7. Azimuthal variation of eigenfunction phase for (*a*) Case A, $m = 0$ and (*b*) Case C, $m = \pm 1$ modes, both seeded at 2500 Hz.

Figure 7 is included to demonstrate that although these two modes have the same radial and streamwise eigenfunction development in accordance with quasi-two-dimensional stability theory, their azimuthal distributions are different and follow their mode type. Shown in this figure is the azimuthal distribution of the mode phase, ϕ_{uf}/π, at each x-position. The subscript uf indicates that the phase was measured between the streamwise velocity fluctuation and a fixed reference time series corresponding to the forcing signal to one of the speakers. For the $m = 0$ mode, we observe the expected constant phase in the azimuthal direction. Contrasting with this, the $m = \pm 1$ mode shows the expected π phase shift across the azimuthal position of the amplitude minimum ($\gamma = 90°$ documented in figure 6*b*).

Based on these comparisons, the thin-shear-layer assumption is clearly validated for this jet. Therefore, the linear stability characteristics of the other forced or interacted modes can be determined on the basis of quasi-two-dimensional instability theory, without concern for their azimuthal wavenumber. In our case this should be valid for at least $m = \pm 4$.

3.2. *Case B*

Representative power spectra of pressure fluctuations at the lip of the jet and velocity fluctuations downstream near the end of the linear region ($x/D = 0.217$) within the shear layer (at the radial location where $U/U_j = 0.6$) are presented for Case B in figure 8. The spectra are shown for two azimuthal positions corresponding to the helical-mode-pair amplitude maximum ($\gamma = 0°$) and minimum ($\gamma = 90°$). The frequency of the forced mode at 1250 Hz is clearly distinguishable and denoted in the figure as f_f.

We have also shown frequencies of unstable modes which have been identified in past experiments (Drubka 1981, see also Drubka, Reisenthel & Nagib 1989; Corke *et al.* 1991; Kusek *et al.* 1990) in this jet under natural conditions. These correspond to the fundamental axisymmetric mode f_0 (2040 Hz), its subharmonic $\frac{1}{2}f_0$ (1020 Hz), and the fundamental helical mode f_1 (2550 *Hz*). Kusek *et al.* (1990, figure 6) have documented a constant St_θ scaling for these modes in this jet for $22\,500 \leqslant Re_D \leqslant$

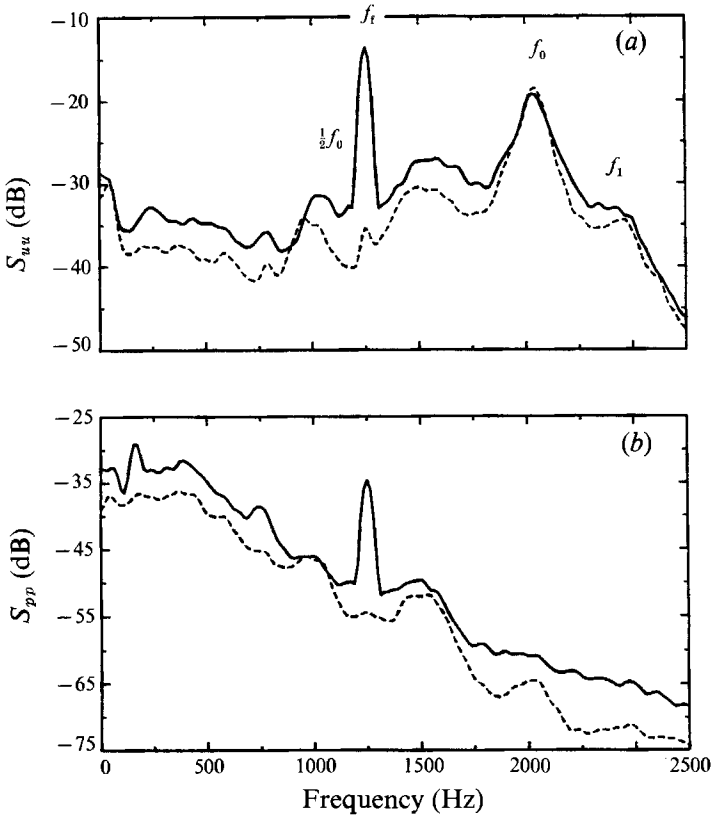

FIGURE 8. Spectra in Case B at two azimuthal locations, corresponding to helical-mode amplitude maximum and minimum for (*a*) velocity fluctuations in the shear layer at $x/D = 0.217$, and (*b*) pressure fluctuations at the exit lip. ——, $\gamma = 0°$ (antinode); – – –, $\gamma = 90°$ (node).

90000. The values of St_θ are 0.0144, 0.0180 and 0.0076 for f_0, f_1 and $\frac{1}{2}f_0$ respectively. The fundamental modes fall on either side of the theoretical most-amplified $St_\theta = 0.017$ determined by Michalke (1971). The mode at $St_\theta = 0.0180$ was determined by Drubka (see Drubka *et al.* 1989, figure 10) to be an $m = \pm 1$ helical mode, based on measurements using a velocity sensor at a fixed position in the shear layer and a pressure sensor monitoring the simultaneous unsteady pressure at the different azimuthal positions on the exit lip. These showed π phase changes in the azimuthal direction associated with the $m = \pm 1$ helical mode.

One might question why the $m = 0$ and $m = \pm 1$ modes appear in the natural jet at different frequencies, since according to the thin-shear-layer approximation which we documented to be valid in this jet, they have identical linear theory characteristics. The explanation, we believe, is due to nonlinear influences further downstream which are transmitted back to the lip of the jet through pressure feedback.

The broad peak in the pressure spectrum and the accompanying small peak in the velocity spectrum at 227 Hz are believed to be due to the instability of the potential core (so-called 'column instability') which scales with the jet diameter (D). In the pressure spectrum at the lip of the jet this represents the largest amplitude, although the amplitude maximum in the velocity fluctuations for the column mode occurs further downstream at $x/D = 3$ to 4. The velocity measurements in figure 8 are at $x/D = 0.217$. Energy at the column-mode frequency occurs at the lip of the jet

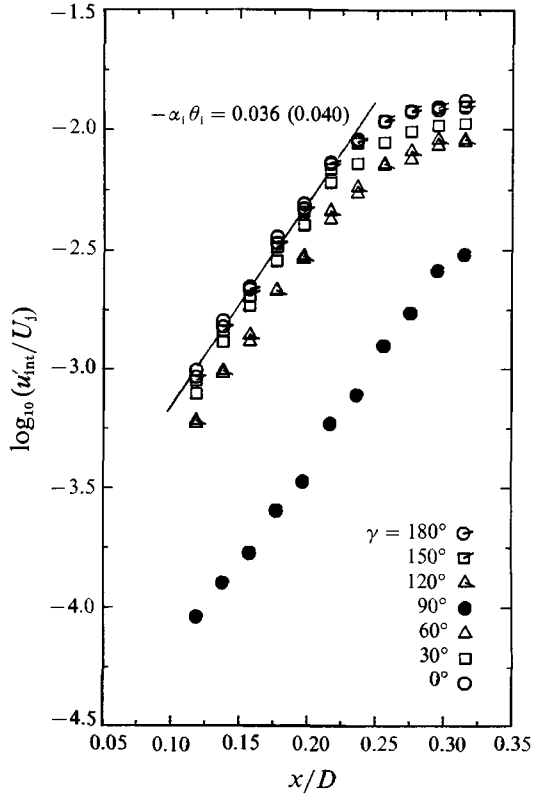

FIGURE 9. Streamwise growth in amplitude of input helical mode in Case B forced at 1250 Hz.

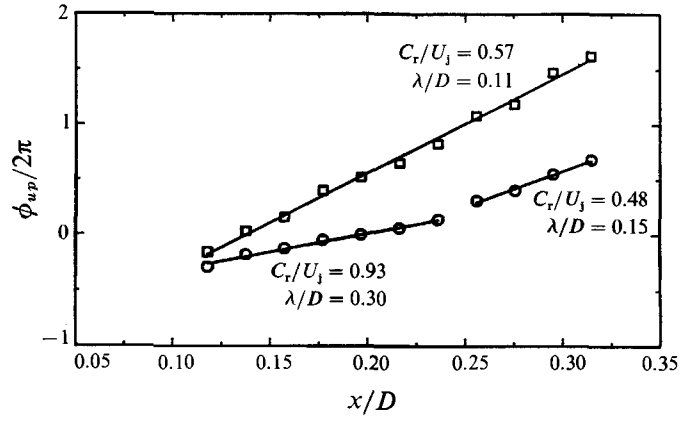

FIGURE 10. Streamwise development of phase for f_0 (□) and f_f (○) modes in Case B.

because of pressure feedback. In this way a shear-layer mode at the column-mode frequency could be self-forced, although it is far from the most linearly amplified frequency for the thin shear layer, and is generally overwhelmed by more amplified modes such as those denoted in this figure.

The streamwise growth in amplitude of the forced mode (f_f) at different azimuthal positions is shown in figure 9. The different initial amplitude levels of this mode with azimuthal position, with a minimum at $\gamma = 90°$, correspond to the $m = \pm 1$ azimuthal

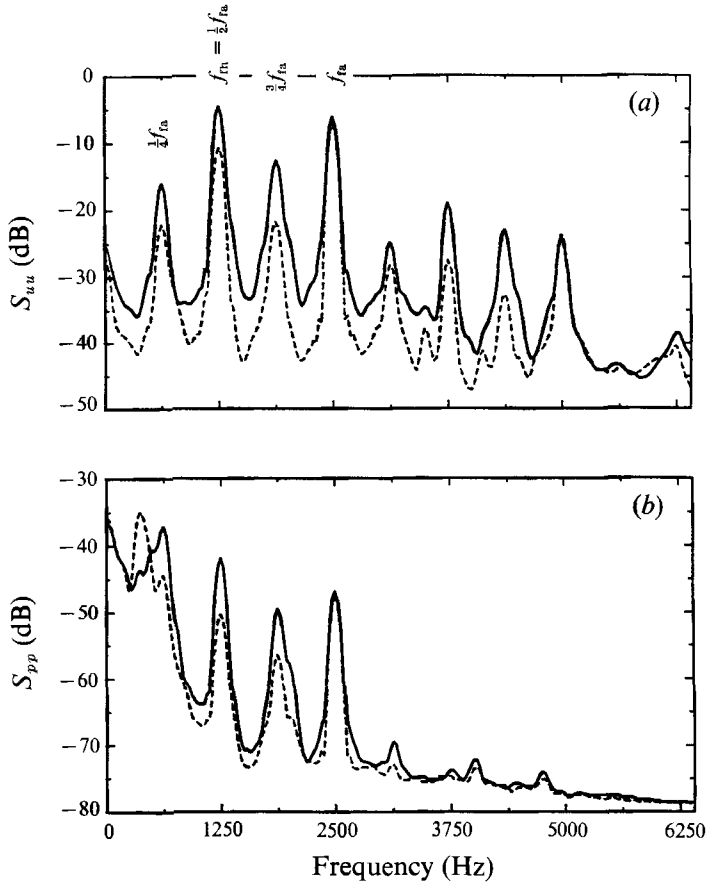

FIGURE 11. Spectra in Case A at two azimuthal locations corresponding to helical-mode amplitude maximum and minimum for (*a*) velocity fluctuations in the shear layer at $x/D = 0.217$ and (*b*) pressure fluctuations at the exit lip. ——, $\gamma = 0°$ (antinode); – – –, $\gamma = 90°$ (node).

wavenumber. Within the linear growth region, a constant spatial amplification rate exists, regardless of the azimuthal position. The value measured here was $-\alpha_i \theta_i = 0.036$. The theoretical value given by Monkewitz & Huerre (1982) is 0.040. Growth curves for the natural fundamental modes in this case (Kusek 1990) showed a similar good comparison to two-dimensional linear theory estimates.

The corresponding downstream development of the phase, ϕ_{up}, for the forced mode is shown in figure 10. These are again taken at the radial position where $U/U_j = 0.6$. The '*up*' subscript indicates that the phase was measured between the streamwise velocity fluctuations at the different x/D positions and simultaneously sampled pressure fluctuations at the exit lip. Also shown for reference is the phase development for the natural axisymmetric mode (f_0). The slope of these lines corresponds to the streamwise wavenumber α_r. The phase velocity is calculated from this as $C_r = 2\pi f/\alpha_r$. Within the linear range, the data document a constant phase velocity for both these modes. For the natural axisymmetric mode, its value is $C_r/U_j = 0.57$. For the forced helical mode, $C_r/U_j = 0.93$. Both correspond well to the linear theory values of 0.65 and 0.85 respectively.

We conclude from figures 9 and 10, and additional evidence compiled by Kusek (1990), that the weakly amplified helical mode that we seeded in this case acts as a passive extra mode which imparts only minor changes in the early evolution of the

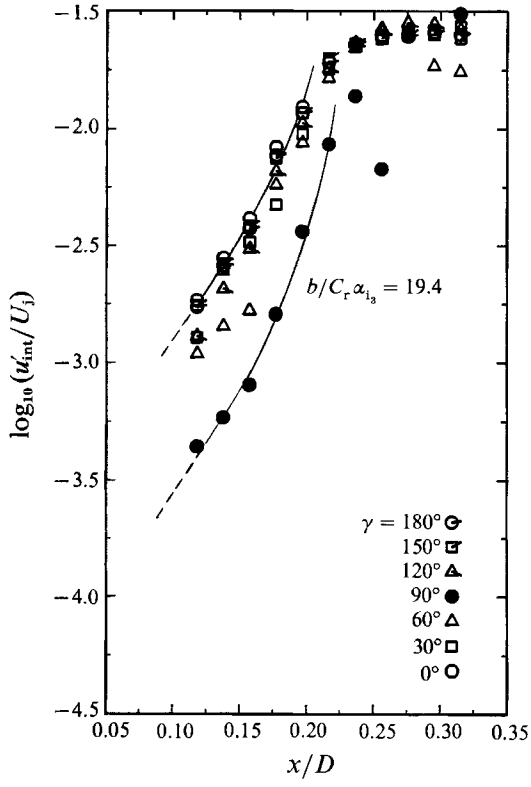

FIGURE 12. Streamwise growth in amplitude of input helical mode in Case A, forced at 1250 Hz.

jet. Thus, it makes a suitable base case for comparison to the condition with an added axisymmetric mode at 2500 Hz (Case A), designed to lead to the resonant growth of the subharmonic helical mode.

3.3. *Case A*

To promote the enhanced growth of the 1250 Hz, $m = \pm 1$ mode of Case B it was superposed with an axisymmetric mode at its harmonic frequency. The outcome of this constitutes the results of Case A. The immediate effect of combining these modes is seen in the velocity and pressure auto-spectra in figure 11. In contrast to the spectra of Case B (figure 8), the natural shear-layer instabilities are now dominated by the two input modes and other modes derived from these. Note that the extent of the frequency axis has been increased in this figure over that for Case B in order to show the energy in higher-frequency modes produced in this case.

Figure 11 shows the spectral peaks corresponding to the two forced modes, the $m = \pm 1$ helical mode, $f_{\rm fh}$, and $m = 0$ mode, $f_{\rm fa}$, as well as two modes which emerge as a result of the forcing, $\frac{1}{4}f_{\rm fa}$ and $\frac{3}{4}f_{\rm fa}$. These spectra peaks are seen to be dominant in both the velocity fluctuations in the shear layer, and pressure fluctuations at the lip of the jet. For the velocity spectra, the spatial location is the same as for the spectra of Case B in figure 8. Also as before, the two line types correspond to two azimuthal positions where the amplitude of the $m = \pm 1$ mode is a maximum and a minimum ($\gamma = 0°$ and 90°, such as seen in figure 2).

The streamwise growth in amplitude of the forced helical mode ($f_{\rm fh}$) at different azimuthal positions is shown in figure 12. This can be contrasted to its counterpart

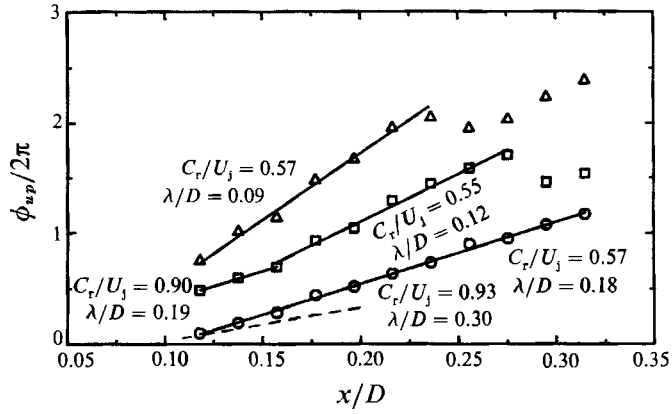

FIGURE 13. Streamwise development of phase for $f_{fa} = 2500$ Hz (△) and $f_{fh} = 1250$ Hz (○) and $\frac{3}{4}f_{fa} = 1875$ Hz (□) modes in Case A. Solid line is a least-squares fit to the data, dashed lined corresponds to linear theory for f_{fh}.

for Case B in figure 9. In particular, we observe that the spatial growth no longer falls on a straight line (exponential growth, $e^{-\alpha_i x}$).

The streamwise development in phase for this mode as well as the forced axisymmetric mode (f_{fa}) are shown in figure 13. For both these modes, the phase points fall on a straight line for $x/D < 0.25$. The slope of these lines corresponds to their streamwise wavenumber, α_r, from which we derive the phase speed of these modes, $C_r = 2\pi f/\alpha_r$. For the axisymmetric mode, the dimensionless phase speed is constant and has a value $C_r/U_j = 0.57$, which agrees well with linear theory.

For the conditions of Case B, the forced helical mode had a phase speed of $C_r/U_j = 0.93$ which agreed with linear theory. The phase development corresponding to that phase speed for that mode is shown as the dashed line in figure 13. In Case A, with the addition of the harmonic axisymmetric mode, the phase speed of the helical mode is substantially lower and matches that of the axisymmetric mode, satisfying the conditions for a resonant energy exchange between them.

In the previous work by Corke *et al.* (1991), the resonant growth of a subharmonic axisymmetric mode was marked by a change in the phase velocity downstream of the first x-measurement station. This was seen as a break in the slope of the linear phase development. Corresponding to this break was an increase in the amplification rate of the subharmonic mode. The streamwise growth of that mode was then represented as two exponential (linear) growth regions, with the upstream portion corresponding to the linear theory value and the downstream portion having a spatial growth greater than predicted from linear theory. An example of this is in figure 16 of Corke *et al.* (1991).

For this case of the subharmonic helical mode, we observe a constant phase speed, without a break, throughout the measured region. As a result, we do not feel justified as before in representing the growth in amplitude of this mode as two exponential regions. Since these modes are phase locked by the first measurement station, where their amplitudes are relatively low, we consider an amplitude evolution model based on a weakly nonlinear three-wave resonance. The three waves in this case are the fundamental axisymmetric mode and subharmonic helical mode pairs. If a_3 and $a_{1,2}$ represent the respective dimensionless amplitudes of these modes, then the amplitude of either helical mode is coupled to that of the axisymmetric mode as

$$da_2/dt = -\sigma_2 a_2 + b a_1^* a_3 + O(a^3),$$

where t is time, σ_2 is the temporal amplification rate (σ_i) of mode 2, b is a coupling coefficient, and * represents the complex conjugate. The origin and a discussion of three-wave resonance leading to this equation is presented by Craik (1985). For the helical modes,

$$a_{1,2} = A_2 \exp\left[\mathrm{i}(\sigma_r + \mathrm{i}\sigma_i)t + \mathrm{i}m\gamma\right]$$

so that $a_1^* = a_2$. In addition, because the phase speeds of the three modes are equal, t can be replaced by x/C_r. Therefore to second order,

$$\mathrm{d}A_2/A_2 = \left(-\alpha_2 + \frac{b}{C_r}A_3\right)\mathrm{d}x,$$

where α_2 is the linear spatial amplification rate of mode 2 (α_i). The amplitude A_3 is that of the axisymmetric mode, which was found to follow linear theory, as shown in figure 6(*b*).

Therefore,

$$\mathrm{d}A_2/A_2 = \left[-\alpha_{i_2} + \frac{b}{C_r}A_{3_0}\exp\left(-\alpha_{i_3}x\right)\right]\mathrm{d}x.$$

Integrating this equation gives a relation for the amplitude of the helical mode in terms of its linear amplification and growth of the axisymmetric mode, namely

$$A_2 = A_{2_0}\exp\left[-\alpha_{i_2}x + b'\exp\left(-\alpha_{i_3}x\right)\right],$$

where $b' = bA_{3_0}/C_r\alpha_{i_3}$, and A_{2_0} and A_{3_0} are reference initial amplitudes for the helical and axisymmetric modes, respectively.

Craik (1985) points out that when the amplitudes of the two waves (helical modes in this case) are small so that there is no back interaction by them on the other wave (the fundamental $m = 0$ mode), then the weakly nonlinear interaction is also usually described as 'parametric resonance'. That this condition is met is evident in figures 6(*a*) and 13, where we observe the streamwise development in amplitude and phase of the fundamental $m = 0$ mode to follow the linear theory development regardless of the presence of the subharmonic helical modes.

We have determined a value for b' from the amplitude data of the helical mode at $\gamma = 90°$, where the initial amplitude is lowest and the neglected $O(a^3)$ terms should be least significant. The values for α_{i_2} and α_{i_3} were the measured values from figures 9 and 6(*a*) respectively. This yielded $b' = 3.76 \times 10^{-2} \pm 2.0 \times 10^{-3}$, or $b/C_r\alpha_{i_3} = 19.41$. Physically we look on this term as a dimensionless coupling coefficient.

Using this value and A_{2_0} as the amplitude of the most-upstream measured data point for $\gamma = 90°$, the amplitude equation is shown as the solid line through the filled points in figure 12. Changing only the value for A_{2_0}, the same equation is drawn for the points at $\gamma = 0°$. For both curves, the dashed line corresponds to the growth of the helical mode based on linear theory.

This evolution equation is observed to represent the growth of the helical mode well in this case, irrespective of the azimuthal position. The equation is valid as long as the neglected terms are insignificant. As the amplitudes grow larger, their influence leads to the amplitude saturation that is observed past $x/D = 0.25$. We have made no attempt to extend the evolution equation to include this region.

Although our primary interest in this case is in the interaction between the fundamental axisymmetric and subharmonic helical modes, we can make some comments on the other dominant modes which appear in the spectrum in figure 11, namely $\frac{1}{4}f_{fa} = \frac{1}{2}f_{fh}$ and $\frac{3}{4}f_{fa}$.

There is possibly more than one scenario to explain the origin of these modes. The difficulty in tracing these is due to pressure feedback by which a mode which might

only naturally develop downstream can appear to originate at the lip of the jet. Corke *et al.* (1991) considered feedback an important element in subharmonic resonance of axisymmetric modes. The fact that the $\frac{1}{4}f_{fa}$ and $\frac{3}{4}f_{fa}$ modes are felt at the lip of the jet is evident by their appearance in the spectra of pressure fluctuations measured there.

As a result of subharmonic resonance in this case, the helical mode, f_{fh} grows at an enhanced rate (according to the double-exponential evolution equation previously presented) and the shear layer rapidly thickens. However, because this mode has an $m = \pm 1$ azimuthal wavenumber, the degree to which the shear layer thickens depends on the azimuthal location. In particular, the maximum spreading occurs at the azimuthal locations of the helical mode amplitude maxima ($\gamma = 0°$ and 180°). This will be further discussed in §3.5. Its relevance to this discussion is to downstream effects, and the origin of additional modes in this case.

With the thickening of the shear layer downstream, according to linear theory the shear layer becomes more unstable to lower frequencies. Of all the possible lower-frequency modes, the subharmonic of the input helical mode would be favoured because it could also interact most efficiently in a weakly nonlinear way. In this scenario, the process for the growth of fluctuations at $\frac{1}{2}f_{fh} = \frac{1}{4}f_{fa}$ would be due to a secondary subharmonic resonance, where the primary mode is the helical mode at f_{fh}, and the basic flow is the azimuthally varying mean flow produced by the initial growth of this mode.

Such a growth of successive subharmonics for axisymmetric modes has been observed in shear layers in jets (see for example the review by Ho & Huerre 1984), where its effect leads to successive pairings of vortices downstream. In this scenario, we might also expect to observe vortex pairing of helical modes. For $m = \pm 1$, this would be most evident at the azimuthal locations of the helical-mode amplitude maxima. This in fact was brought out in our earlier work (Kusek, Corke & Reisenthel 1989). In particular, when we introduced $m = \pm 1$ helical modes near their most-amplified frequency, and with sufficient initial amplitude so that they would dominate over other instability modes, flow visualization documented that downstream the streamwise wavelength of the helical mode would double compared to the initial value. This came about as a disconnection of the helical modes near the azimuthal locations of amplitude minima, and vortex pairing at locations of amplitude maxima.

A sample from that early work is shown in figure 14(*a*). In this case $Re_D = 20000$, and the flow direction is from left to right. The smoke was introduced into the shear layer as a circular sheet all around the circumference of the jet exit. It was illuminated with a short-duration strobe lamp. Figures 14(*a*) and 14(*b*) correspond to the azimuthal locations of the amplitude maxima of the helical mode. From this viewpoint the staggered formation of vortices is indicative of the $m = \pm 1$ helical mode. Pairing appears to occur on the top row of vortices, two wavelengths from the left edge of the photograph. Downstream of this point we observe a doubling of the initial wavelength.

In the present case with combined subharmonic $m = \pm 1$ helical and fundamental $m = 0$ modes, flow visualization also provides evidence of vortex pairing further downstream. A sample is shown in figure 14(*b*). In this case $Re_D = 4000$; however, the frequencies of the two input modes were reduced so that their Strouhal numbers, $St_\theta = f\theta/U_j$ remained the same as for Case A. The method for performing the flow visualization and the viewpoint are the same as for figure 14(*a*). In this case we use arrows to mark the approximate locations of the centres of the top row of vortices.

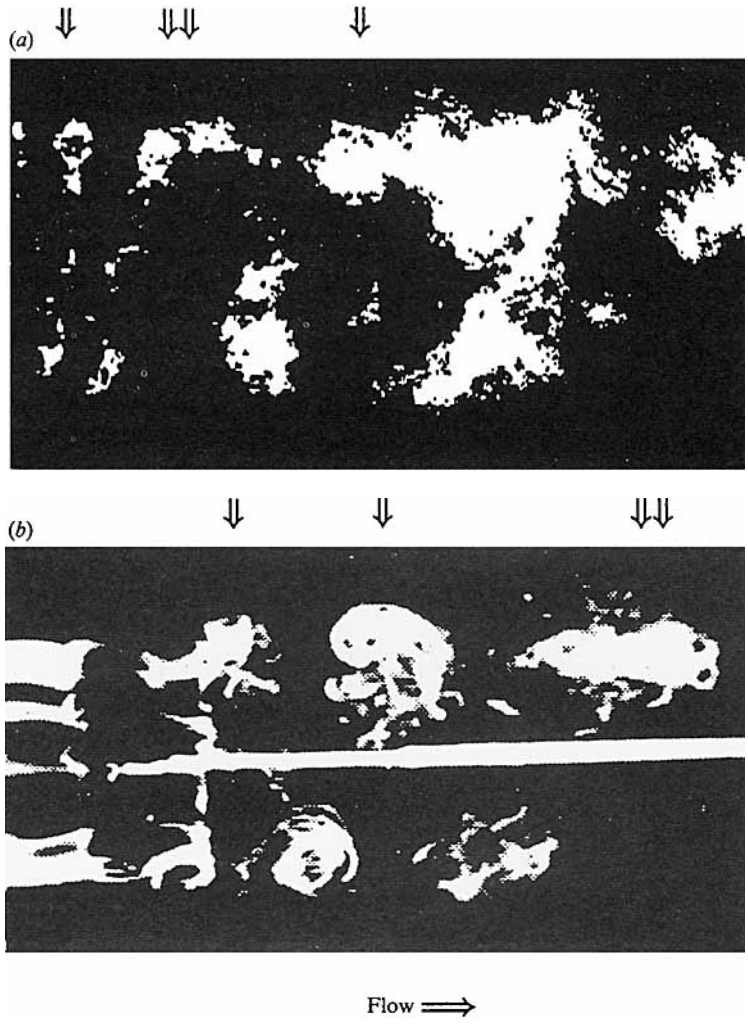

FIGURE 14. Smoke-wire flow visualization of the jet shear layer for different conditions with $m = \pm 1$ helical-mode input that demonstrate helical-mode vortex pairing. (*a*) $Re_D = 20000$ with a helical-mode input at its most unstable frequency (from Kusek *et al.* 1989). (*b*) $Re_D = 4000$ with $m = 0$ mode input at most-amplified frequency and $m = \pm 1$ mode at its subharmonic frequency.

The first vortex rollup is expected to closely correspond to the location of energy saturation of the subharmonic helical mode. The distance between the first two vortices gives the initial streamwise wavelength of the helical mode. Further downstream, the elongated structure double arrows and increased streamwise wavelength suggest that vortex pairing may also be taking place in this case.

We note that in this process, the mode that results after pairing is also helical, with the same (± 1) azimuthal wavenumber. This observation agrees with the spectra in figure 11 which show an azimuthal variation in amplitude at $\frac{1}{2}f_{\mathrm{fa}}$ which is consistent with an $m = \pm 1$ mode.

Although pairing would take place downstream of our last measurement station, its effect could be felt back at the lip of the jet due to pressure feedback. Pressure

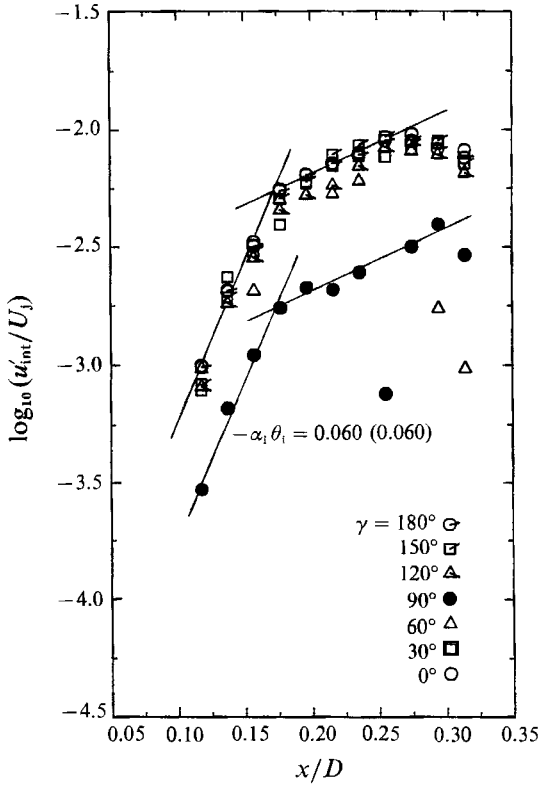

FIGURE 15. Streamwise growth in amplitude of $\frac{3}{4}f_{\rm fa} = 1875$ Hz mode in Case A.

feedback from the site of the first vortex pairing of axisymmetric modes was previously confirmed by Corke *et al.* (1991). We expect the process to be similar here. In the initial region, the mode at $\frac{1}{4}f_{\rm fa}$ would be forced by feedback at the lip and grow according to linear theory. At that location where the shear layer is thin, it would be relatively weakly amplified. However, its initial amplitude is not insignificant and its presence, along with the two input modes, is capable of producing through sum and difference interactions the other modes observed in the spectrum in figure 11.

If this scenario is correct, the $\frac{3}{4}f_{\rm fa}$ mode could be produced by either $f_{\rm fa}-\frac{1}{4}f_{\rm fa}$ or $f_{\rm fh}+\frac{1}{4}f_{\rm fa}$. For the former, the azimuthal wavenumber of the mode produced would be ± 1. For the latter, it would be ± 2. The streamwise growth in amplitude of the $\frac{3}{4}f_{\rm fa}$ mode at different azimuthal positions is shown in figure 15. At any x/D location, the variation in amplitude with azimuthal position confirms $m = \pm 1$ for this mode.

Figure 15 along with the phase development of $\frac{3}{4}f_{\rm fa}$ in figure 13 document the initial evolution of this mode. As a result of the difference interaction $(f_{\rm fa}-\frac{1}{4}f_{\rm fa})$, this mode is essentially forced at the lip of the jet. From the exit lip to approximately $x/D = 0.17$, this mode grows according to linear theory. This is confirmed by both its growth rate and phase velocity determined from these two figures. Past this x-position, we observe an abrupt decrease in the phase speed of this mode, accompanied by a sharp decrease in its amplification rate. Because of the break in the phase development, we have represented the amplitude development as two linear growth regions. Past $x/D = 0.25$, the amplitude in this mode saturates and decays.

Based on these observations it would appear that the $\frac{3}{4}f_{\rm fa}$ mode is produced at the lip of the jet. In the initial thin shear layer it is relatively highly amplified. However,

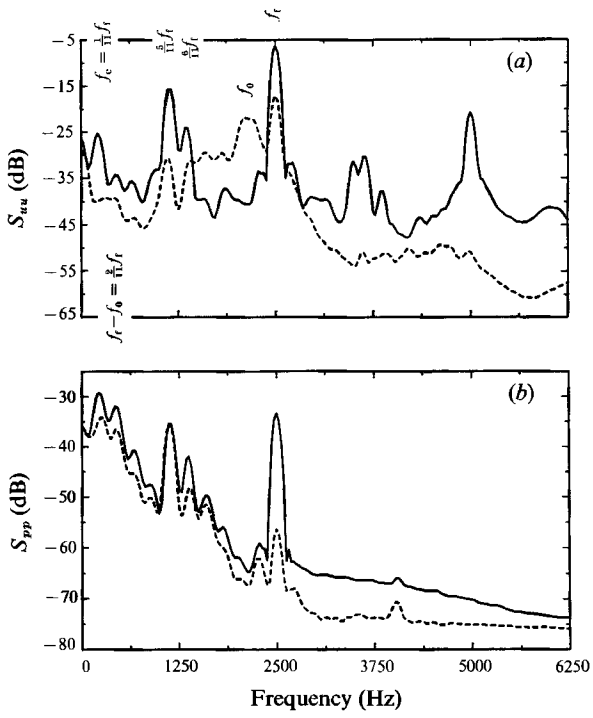

FIGURE 16. Spectra in Case C at two azimuthal locations corresponding to helical-mode amplitude maximum and minimum for (*a*) velocity fluctuations in the shear layer at $x/D = 0.217$ and (*b*) pressure fluctuations at the exit lip. ——, $\gamma = 0$ (antinode); – – –, $\gamma = 90°$ (node).

the secondary growth of the subharmonic helical mode leads to a rapid growth of the shear layer. From a linear stability standpoint, as the shear layer thickens, the most-amplified frequencies shift towards lower values. It appears that in this process the $\frac{3}{4}f_{fa}$ mode becomes less amplified downstream and behaves more or less only as a passive additive mode.

3.4. *Case C*

As pointed out in §2.1, the conditions of this case were meant to produce a counterpart to the forced case at $Re_D = 70000$ in Corke *et al.* (1991), whereby the same frequency was used, but an $m = \pm 1$ helical mode was input rather than an $m = 0$ mode. The frequency of the input mode is near the most-amplified one with $St_\theta = 0.018$, where 0.017 is most amplified according to linear theory. As was demonstrated in §3.1, because the initial shear layer is thin the differences between the linear stability characteristics of the $m = 0$ and $m = \pm 1$ modes are insignificant.

The results of this input condition were identical with those of Corke *et al.* (1991), namely the appearance of $\frac{1}{11}$th-based combinations of the forced mode (f_f). With this, instead of an exact subharmonic, there appeared near-subharmonic values of $\frac{5}{11}f_f$ and $\frac{6}{11}f_f$. Velocity spectra at $x/D = 0.217$ and pressure spectra at the lip of the jet showing this are shown in figure 16. As before, the solid curve corresponds to an azimuthal location of the input helical-mode amplitude maximum, and the dashed curve to the location of an amplitude minimum. At the latter azimuthal position, we note the appearance of a peak in the spectrum at the frequency of the natural (unforced) axisymmetric mode ($f_0 = 2040$ Hz). This peak appears to be completely suppressed at the position of the helical-mode amplitude maximum.

In order to understand the origin of the modes in this case, we have concentrated

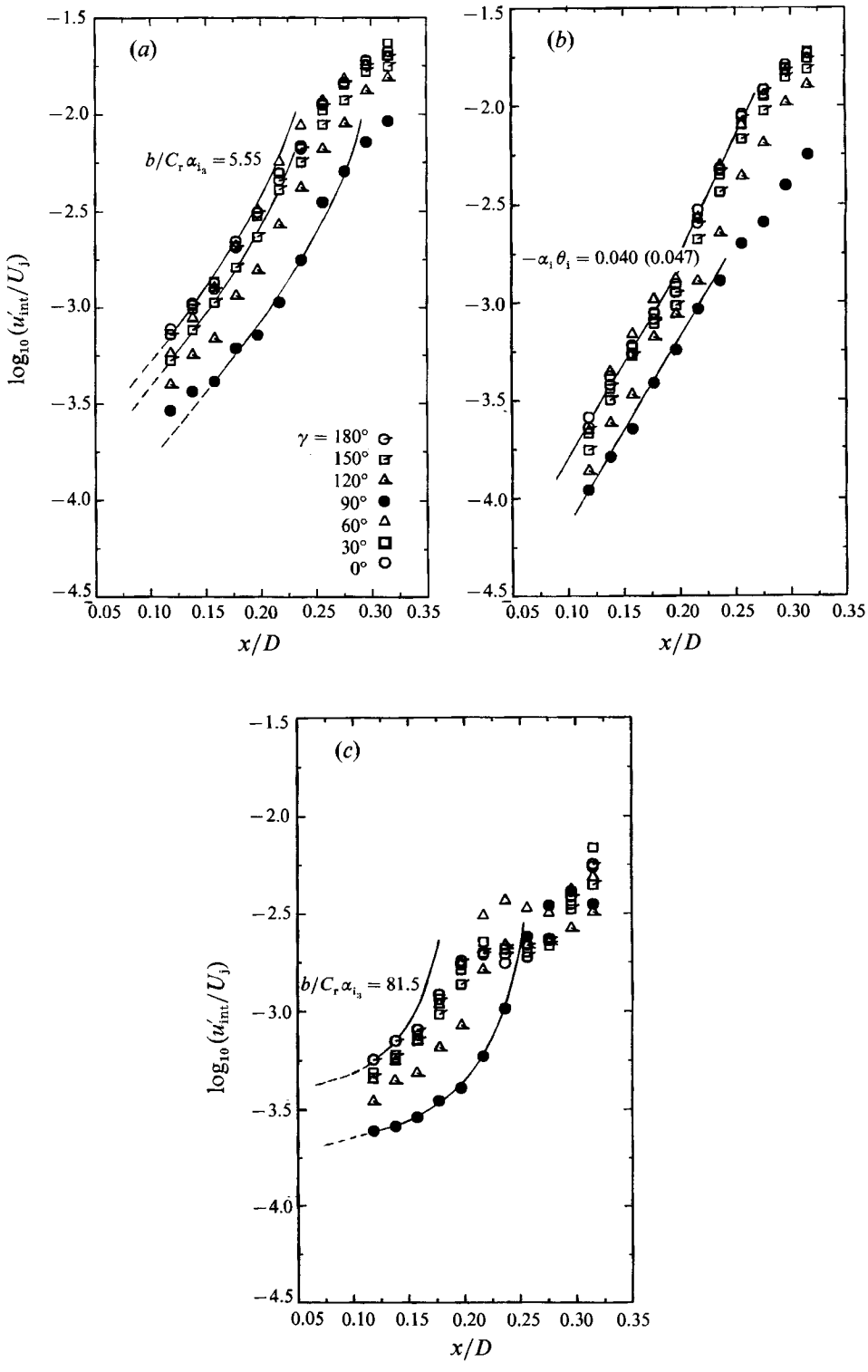

FIGURE 17. Streamwise growth in amplitude of $\frac{5}{11}f_t$ = 1136 Hz (*a*), $\frac{6}{11}f_t$ = 1364 Hz (*b*), $\frac{1}{11}f_t$ = 227 Hz (*c*) modes in Case C.

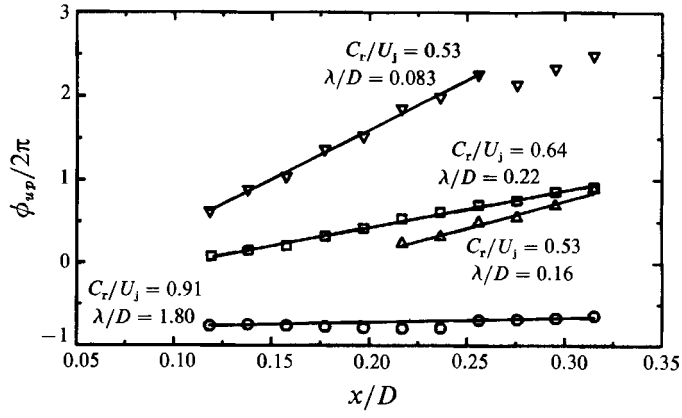

FIGURE 18. Streamwise development of phase in $f_t = 2500$ Hz (∇), $\frac{1}{11}f_t = 227$ Hz (○), $\frac{5}{11}f_t$ (□), $\frac{6}{11}f_t = 1364$ Hz modes in Case C.

on the following frequencies in detail: f_t, $\frac{5}{11}f_t$, $\frac{6}{11}f_t$, $\frac{1}{11}f_t$ and f_0. The streamwise growth in amplitude for f_t, is presented in figure 6(*b*). The phase speed was determined from figure 18 (downward triangle) to have the constant value of $C_r/U_j = 0.53$. These confirmed that this mode was developing according to linear theory. Similar measurements (not presented) showed that the mode at f_0 also developed according to linear theory with a constant amplification rate of $-\alpha_i\theta_i = 0.058$ and a constant phase speed of $C_r/U_j = 0.57$. Both these matched the values measured for f_0 under the conditions of Case B, for example in figure 10.

The streamwise development in amplitude and phase of the $\frac{5}{11}f_t$, $\frac{6}{11}f_t$ and $\frac{1}{11}f_t$ modes is presented in figures 17 and 18. We consider first the $\frac{5}{11}f_t$ mode, which Corke *et al.* (1991) had concluded resulted from the same subharmonic resonance mechanism that leads to pairing in natural jet shear layers, such as shown here for the enhanced growth of the subharmonic helical mode in Case A. Our conclusion is the same, based on the similarities between the streamwise development of the $\frac{5}{11}f_t$ mode here and the subharmonic mode (f_{th}) of Case A.

The first similarity which leads us to this conclusion is that this mode has a constant phase speed throughout the measurement region which is significantly lower than the linear theory value and close to that of the near-fundamental mode. The streamwise wavenumber, α_r, was determined from the slope of the linear curve fit through the measured phase values (square symbols) in figure 18. From this, the dimensionless phase speed was calculated to be $C_r/U_j = 0.60$. The linear theory value is 0.78.

As a result of the constant and nearly matched phase speeds of the f_t and $\frac{5}{11}f_t$ modes, we expect to find an enhanced growth of $\frac{5}{11}f_t$ through a weakly nonlinear interaction similar to that in Case A. A similar near-subharmonic/fundamental resonance exists in boundary layers, which is referred to as 'combination resonance' by Santos & Herbert (1986, see also Herbert 1988). Also for boundary layers, Corke (1990) referred to this as 'detuned resonance'. We believe that the enhanced growth of the $\frac{5}{11}f_t$ mode in this case is another example of this. In all these cases, the resonant interaction does not require a matching of frequencies but rather a close (but not necessarily exact) matching of phase speeds.

The downstream growth in amplitude of the $\frac{5}{11}f_t$ mode for different azimuthal positions is shown in figure 17(*a*). The change in the initial amplitude level with azimuthal position confirms that $m = \pm 1$ for this mode. As with the subharmonic

mode in Case A, we have applied the amplitude evolution equation to the data and determined the coefficient b'. As previously done, the value of b' was determined for only one γ-position and then compared to the amplitude data at the other γ-positions. The data we chose to use was at $\gamma = 150°$ (flagged-square symbols). These were selected because the initial points more closely followed linear theory. The linear growth with $-\alpha_i \theta_i = 0.033$ is shown as the dashed line in the figure.

Based on this data set, $b' = bA_{3_0}/C_r \alpha_{i_3}$ was $8.01 \times 10^{-3} \pm 2.7 \times 10^{-3}$. Using the initial amplitude for the fundamental mode at $\gamma = 150°$, the dimensionless coupling coefficient, $b/C_r \alpha_{i_3}$, was 5.55 ± 1.9. The amplitude equation using this coefficient is shown as the solid line through the $\gamma = 150°$ data points.

One of the basic differences between this case and Case A is that here the fundamental mode is helical with $m = \pm 1$. Therefore the initial amplitude, A_{3_0}, varies with the azimuthal position (such as in figure 2). We apply the evolution equation, changing only the initial amplitudes, to obtain the solid curves appropriate to $\gamma = 0°$ (open circles) and 90° (filled circles).

Examining the results, we find that the amplitude equation represents the enhanced growth of the $\frac{5}{11}f_f$ mode reasonably well, especially near the azimuthal positions of the $\frac{5}{11}f_f$ amplitude maxima. The impact of the γ-variation of the initial amplitude of the fundamental mode (f_f) is to produce larger growth rates near the azimuthal positions of initial amplitude maxima (0° and 180°) than at the minima (90°). This is clearly evident from the data, by simply translating downward the curve at $\gamma = 0$ over the data points for $\gamma = 90°$. The amplitude model captures this behaviour well.

We find in this case that the coupling coefficient, $b/C_r \alpha_{i_3}$, was approximately 3.5 times smaller than the value determined in Case A. This seems consistent with the idea that the energy exchange is not as efficient in this case owing to the less perfect matching of phase speeds between modes. However, in general it appears that the physical process is the same and accounts for the rapid growth of the $\frac{5}{11}f_f$ mode.

Corke *et al.* (1991) had observed the $\frac{6}{11}f_f$ mode to develop downstream according to linear theory. In an initial region up to $x/D = 0.2$, we find a similar result. This can be seen in terms of the amplitude development of this mode in figure 17(*b*). The straight line corresponds to the amplification rate of $-\alpha_i \theta_i = 0.040$ which compares to the linear theory value of 0.047. Within this region for this mode, the linear coherence between the pressure fluctuations at the lip of the jet and velocity fluctuations downstream in the shear layer always fell below 0.5, which is our threshold for accurate phase measurements. The same type of insignificant level of linear coherence was also found for this frequency by Corke *et al.* (1991). As a result, we could not determine the phase speed of this mode in this region.

Past $x/D = 0.2$, we observed a sharp increase in the amplification rate of the $\frac{6}{11}f_f$ mode. Coincident with this was an increase in the linear coherence above our threshold value. In this region we were then able to determine the phase development of this mode. The values are shown in figure 18 (upward triangles). The phase speed in this region corresponding to these values is constant and equal to $C_r/U_j = 0.53$. This phase speed is, then, considerably slower than its linear theory value of 0.75, and matches at this point the value for the input mode f_f.

It appears that the streamwise development of the $\frac{6}{11}f_f$ mode is not unlike that of the $\frac{3}{4}f_f$ mode in Case A; that is, it starts as an essentially passive linear additive mode. Only further downstream, with the growth in amplitude of the input, f_f, and $\frac{5}{11}f_f$ modes, and the growth in the shear-layer thickness, it is able to couple with f_f. At that point it achieves some enhanced growth.

The downstream development of the $\frac{1}{11}f_f$ mode is shown in terms of amplitude in figure 17(*c*), and phase as the circular symbols in figure 18. Regarding the phase, the phase speed is constant, with a value of $C_r/U_j = 0.91$. This compares to the linear theory value of 0.97. For the amplitude, the variation in the initial level with azimuthal position confirms that the $\frac{1}{11}f_f$ mode has $m = \pm 1$. The linear theory value for the growth in amplitude is shown as the dashed line. At the $\gamma = 90°$ position, the initial growth is close to linear. However, further downstream and for all the other γ-positions, an enhanced amplification similar to the $\frac{5}{11}f_f$ mode is observed. Because of this similarity, we applied the same amplitude model and determined a coupling coefficient between the $\frac{1}{11}f_f$ and f_f modes, utilizing the amplitude values for $\gamma = 90°$. The resulting amplitude curve is shown as the solid line through the filled-circular symbols. For this, the dimensionless coupling coefficient was found to be 81.5 ± 7.5. The amplitude model represented the growth at this γ-location quite well. We applied this same function to the $\gamma = 0°$ position while only adjusting for the azimuthal change in the initial amplitudes of the two modes. This is shown as the solid line through the open-circular symbols. In this case, the amplitude equation overpredicts the growth of this mode.

For the $\frac{1}{11}f_f$ mode, we had tried using the linearly growing $\frac{2}{11}f_f$ mode as the fundamental in the weakly nonlinear model. However, this was found to greatly under predict the growth of $\frac{1}{11}f_f$. Only the use of the more-amplified linear mode (f_f) could account for the larger growth in amplitude of $\frac{1}{11}f_f$. Also, strictly speaking, one should include the amplitude development of other modes such as $\frac{10}{11}f_f$ and $\frac{12}{11}f_f$ which can sum or difference with f_f to produce $\frac{1}{11}f_f$. However, figure 16 showed that the amplitudes of these frequency sidebands to the fundamental mode are insignificant (nearly 30 dB lower than f_f) so that their contributions to the growth of $\frac{1}{11}f_f$ must be minimal.

What is the origin of the $\frac{1}{11}f_f$ based modes in Case C? It is not due to the method by which we introduced the disturbances, since the same result occurred for Corke *et al.* (1991) when using far-field sound.

In an independent study in the same facility, Reisenthel *et al.* (1991) had investigated the characteristics of the instability mode which scales with the jet exit diameter (the so-called 'jet column mode'). Because this mode and the shear-layer modes have characteristic scales, D and θ respectively, and because D/θ is generally of the order of 10^2 (approximately 500 in our case), the instability frequencies associated with these differ considerably. In a natural jet, the column mode does not generally have a significant role in the initial development of the flow. However, conditions such as Drubka's $Re_D = 42000$ jet (see Drubka *et al.* 1989) indicate that it can, when an integer number of successive subharmonic frequency reductions of the initial shear-layer mode leads to a matching downstream to the column-mode frequency. Under those conditions, the pressure fluctuations corresponding to the first subharmonic were extra strongly felt at the lip of the jet, providing self-forcing and suggesting to some degree a global resonance.

Under natural jet conditions for a fixed Reynolds number, Reisenthel *et al.* (1991) found that the Strouhal number of the column mode decreased with downstream distance, falling in a range from $0.6 < St_D < 0.4$ for $0.5 < x/D < 6.0$. This brackets the range of values tabulated by Gutmark & Ho (1983) for different jet facilities. In the light of this result, with respect to the column-mode instability the $\frac{1}{11}f_f$ mode corresponds to $St_D = 0.54$, which places it in the most-amplified frequency region.

In general it appeared that the modes that were multiples of $\frac{2}{11}f_f$ developed essentially as linear additive modes. In contrast, the modes that were derived by an

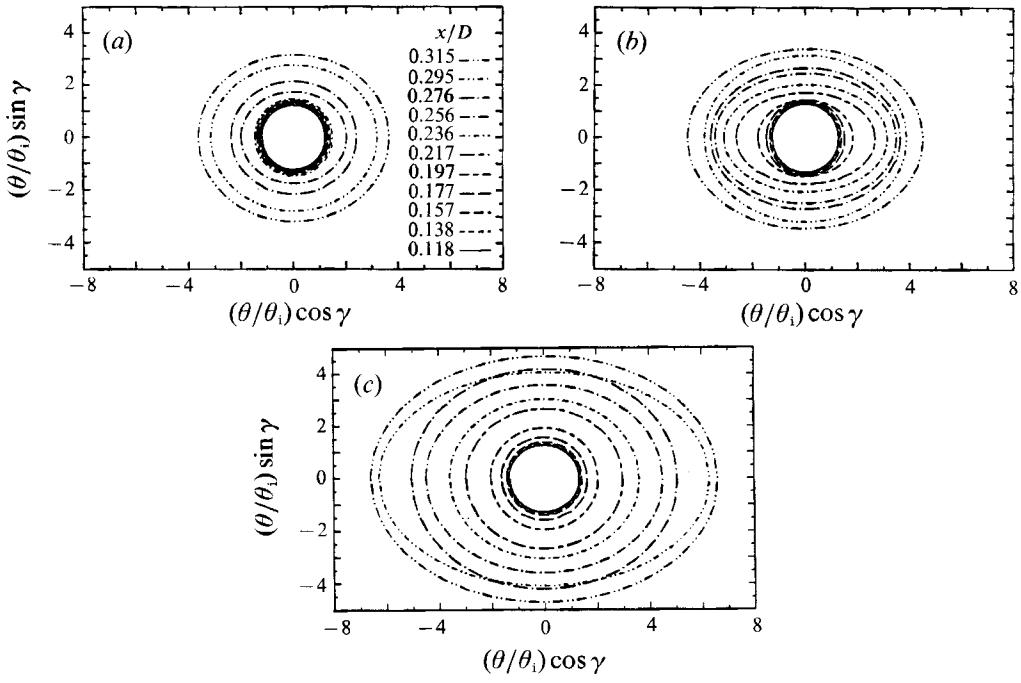

FIGURE 19. Streamwise development of azimuthal variation in momentum thickness in Cases B (*a*), C (*b*) and A (*c*).

interaction with $\frac{1}{11}f_t$ grew at an enhanced rate. The fact that the frequencies of all these modes appear in the spectrum of pressure fluctuations at the lip of the jet indicates that they are to some degree self-forced. Except for the input mode, all the other modes had to originate from interactions that occurred downstream, communicated back to the jet lip by pressure feedback. Such a downstream influence can account for the fine tuning of these modes which is exhibited by the sharp spectral peaks.

3.5. *Mean flow effects*

The effect of the three input conditions (A, B, C) on the mean flow is presented in figures 19 and 20. In figure 19, we show this from a viewpoint which illustrates the azimuthal variation of the momentum thickness at different x-positions. We construct this with a two-dimensional polar coordinate system, where at any x-location the local radius equals the normalized momentum thickness, $\theta(x,\gamma)/\theta_i$. For clarity, rather than showing the discrete points, we show a curve which is the result of the best fit of the data to a general, origin-centred ellipse. In the fit, we assumed a horizontal symmetry plane. The different x-positions are denoted by different line types. In this representation, the azimuthal locations of the amplitude maxima for the input $m = \pm 1$ modes are on a line parallel with the abscissa.

When the helical mode grows to large amplitude, we expect a nonlinear interaction to result in the modification of the mean flow. For helical-mode pairs with azimuthal wavenumbers $\pm m$ and streamwise wavenumber α_r, the difference interaction $(\alpha_r, \pm m) - (\alpha_r, \pm m) = (0, \pm 2m)$ produces an azimuthal variation of the mean flow with azimuthal wavenumber $\pm 2m$. Physically, this will appear as a $\cos 2\gamma$ variation of the shear-layer thickness (see for example Long & Peterson 1992). From the viewpoint used in figure 19, this will appear as an ellipse-shaped distribution of the

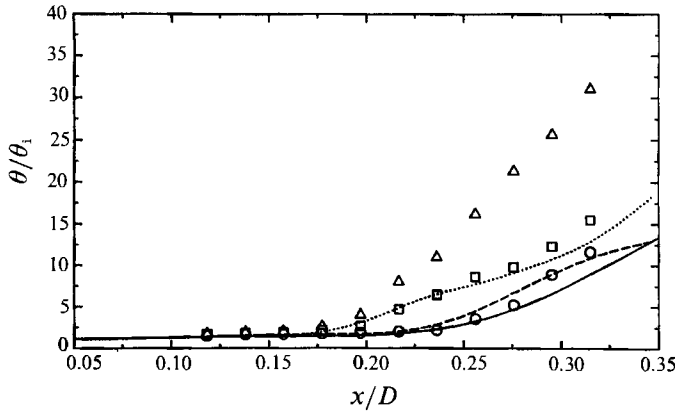

FIGURE 20. Streamwise development of azimuthally summed momentum thickness for three cases (Case A (△), Case B (○), Case C (□)); and unforced jet (——) and two $m = 0$ forced cases (2050 Hz (– – –) and 2500 Hz (· · · · ·)) from Corke *et al.* (1991).

momentum thickness. The degree of eccentricity above one is a measure of the amount of mean flow distortion resulting from the growth of the helical modes.

The momentum thickness distribution for the base flow case (B) is shown in figure 19(*a*). Upstream of $x/D = 0.25$, the azimuthal distribution is circular, indicating that the weakly amplified helical mode input in this case is not of sufficient amplitude to distort the mean flow. Further downstream of this point, the amplitude reached by this mode does result in a small degree of eccentricity, with a maximum value of 1.15 by the last x/D-position.

The momentum-thickness distribution for the conditions to promote the resonant growth of the subharmonic helical mode (Case A) is shown in figure 19(*c*). In this case, the rapid growth in amplitude of the helical mode produces a noticeable azimuthal mean flow distortion by the first measurement station. By the last x-location the value of the eccentricity in the mean flow is 1.50.

For the near-subharmonic resonant case (C), the momentum thickness distribution is shown in the middle of figure 19(*b*). In this case the growth in amplitude of the helical mode at $\frac{5}{11}f_t$ is somewhat slower than for the exact subharmonic in Case A, so that the first indication of an azimuthal distortion of the mean flow occurs somewhat downstream at $x/D = 0.177$. Also, the spreading of the momentum thickness is visibly less in this case than in Case A, although the maximum eccentricity reached is the same.

In order to get a quantitative comparison of the total growth of the momentum thickness among the three cases, the areas of the fitted ellipsi were determined and plotted in figure 20. Included in the figure is the growth of the momentum thickness in the natural (unforced) jet, and in the jet with $m = 0$ mode forcing comparable to Cases A and C, which were taken from Corke *et al.* (1991). For the natural jet and $m = 0$ forced cases, we assumed that the azimuthal distribution was circular.

Comparing Cases A–C and the unforced jet shows a consistent pattern. In Case B, the addition of the weakly amplified helical mode had in general little effect on the spreading of the jet. This is evident from the overlap of the Case B values on the solid curve up to $x/D = 0.25$.

The near-subharmonic helical-mode resonance in Case C led to a more enhanced growth of the momentum thickness over the natural jet. By the last x/D-position, the azimuthally summed momentum thickness was 50% larger. By far the largest

growth in the momentum thickness occurred for exact subharmonic resonance in Case A. By the last x/D-location, the azimuthally summed momentum thickness was twice as large as that in Case C, and three times that of the natural jet.

In order to document the initial linear and weakly nonlinear behaviour, we have confined our measurements to be within a few wavelengths of the jet exit lip. We expect that the major impact of the helical-mode seeding on the jet evolution will occur even further downstream of our measurement stations. In the path to turbulence, the development of three-dimensionality is the inevitable outcome. The helical-mode resonance documented here allows a mechanism for the early introduction of coherent three-dimensional modes, and suggests a scenario for the early evolution of turbulent jets.

4. Conclusions

Confirmation of quasi-two-dimensional linear theory predictions of the relative insensitivity of amplification rates and phase velocities to azimuthal wavenumber, m, came from comparisons between forced modes with $m = 0$ and $m \pm 1$, at the same streamwise wavenumber. These compared well with each other, as well as with linear theory predictions. The shear-layer curvature parameter in these cases was $r_{\frac{1}{2}}/\theta_i = 260$. The analysis of Ahmadi-Moghadam (1986) had predicted an insensitivity to azimuthal wavenumber up to $m = \pm 4$ for $r_{\frac{1}{2}}/\theta_i = 100$. From our results, we expect to be able to excite helical modes up to $m = \pm 6$, the limit of the 12 speaker arrangement.

By the proper selection of streamwise wavenumbers of $m = \pm 1$ helical modes with and without a simultaneously forced axisymmetric mode, the forced jet's developing shear layer exhibited very different modal compositions and downstream development. The first case (B) consisted of a weakly amplified (from a linear stability point of view) $m = \pm 1$ mode at a low initial amplitude. It was found to act as a passive additive mode which did not interact with or overwhelm the other natural instability modes. As such, this case provided a reference for the second case (A) where, in addition to the $m = \pm 1$ mode, an $m = 0$ mode at the harmonic frequency was added. The combination of these two lead to the resonant growth of the subharmonic helical mode. A weakly nonlinear three-wave amplitude evolution equation with a coupling coefficient derived from the data was found to model the enhanced growth of the subharmonic mode well.

The last case (C) was meant to be a counterpart of the $Re_D = 70000$ forced case of Corke *et al.* (1991) whereby an input $m = \pm 1$ mode was substituted for an $m = 0$ mode. The frequency of the input mode was the same and near the most-amplified value based on linear theory. This input had the identical effect to the previous work, in that it led to the appearance of $\frac{1}{11}$th-based combinations of the forcing frequency (f_f), with near-subharmonic values of $\frac{5}{11}f_f$ and $\frac{6}{11}f_v$ appearing. The results confirmed the resonant amplification of the $\frac{5}{11}f_f$ mode. This was also well represented by the weakly nonlinear amplitude equation, including the dependence of the streamwise amplification rate on the azimuthal change in the fundamental-mode initial amplitude. The coupling coefficient in this case was approximately one-third that for exact fundamental–subharmonic resonance in Case A.

Finally, in both cases with resonant helical mode growth (C and A) we documented a $\cos 2\gamma$ azimuthal variation of the mean flow which was attributable to a difference interaction between the $m = \pm 1$ helical modes. The azimuthally summed momentum thickness for conditions of exact subharmonic resonance was 300% larger than in the

unforced jet. This was measured only three fundamental-mode wavelengths downstream of the jet exit. The slope of the growth indicates a potential increase further downstream of that point.

We would like to acknowledge the helpful input of Professor Thorwald Herbert regarding the theoretical aspects of this work. This work was supported by a grant from the Air Force Office of Scientific Research, No. 90-0173, which is monitored by Dr James McMichael.

REFERENCES

AHMADI-MOGHADAM, A. 1986 On the instability of thin circular shear layers. Ph.D. thesis, Illinois Institute of Technology, Chicago.

COHEN, J. & WYGNANSKI, I. J. 1987*a* The evolution of instabilities in the axisymmetric jet. Part 1. The linear growth of disturbances near the nozzle. *J. Fluid Mech.* **176**, 191–219.

COHEN, J. & WYGNANSKI, I. J. 1987*b* The evolution of instabilities in the axisymmetric jet. Part 2. The flow resulting from the interaction between waves. *J. Fluid Mech.* **176**, 221–235.

CORKE, T. 1980 Effect of controlled resonant interactions and mode detuning on turbulent transition in boundary layers. In *Laminar-Turbulent Transition* (ed. R. Eppler & H. Fasel), pp. 151–178. Springer.

CORKE, T. C., KRULL, J. D. & GHASSEMI, M. 1992 Three dimensional mode resonance in far wakes. *J. Fluid Mech.* **239**, 99–132.

CORKE, T. C., SHAKIB, F. & NAGIB, H. M. 1985 Effects of low amplitude forcing on axisymmetric jet flows. *AIAA Paper* 85-0573.

CORKE, T. C., SHAKIB, F. & NAGIB, H. M. 1991 Mode selection and resonant phase locking in unstable axisymmetric jets. *J. Fluid Mech.* **223**, 253–311.

CRAIK, A. D. D. 1985 *Wave Interactions and Fluid Flows.* Cambridge University Press.

DRUBKA, R. E. 1981 Instability in the near field of turbulent jets and their dependence on initial conditions and Reynolds number. Ph.D. thesis, Illinois Institute of Technology, Chicago.

DRUBKA, R. E., REISENTHEL, P. & NAGIB, H. M. 1989 The dynamics of low initial disturbance turbulent jets. *Phys. Fluids* A**1**, 1723–1735.

GUTMARK, E. & HO, C.-M. 1983 Preferred modes and the spreading rates of jets. *Phys. Fluids* **26**, 2932–2938.

HERBERT, TH. 1988 Secondary instabilities of boundary layers. *Ann. Rev. Fluid Mech.* **20**, 487–526.

HO, C.-M. & HUERRE, P. 1984 Perturbed free shear layers. *Ann. Rev. Fluid Mech.* **16**, 364–424.

KUSEK, S. M. 1990 Helical instability modes in jets. M.S. thesis, Illinois Institute of Technology, Chicago.

KUSEK, S. M., CORKE, T. C. & REISENTHEL, P. 1989 Control of two and three dimensional modes in the initial region of an axisymmetric jet. *AIAA Paper* 89-0968.

KUSEK, S. M., CORKE, T. C. & REISENTHEL, P. 1990 Seeding of helical modes in the initial region of an axisymmetric jet. *Exps Fluids* **10**, 116–124.

LONG, T. A. & PETERSON, R. A. 1992 Controlled interactions in a forced axisymmetric jet. Part 1. *J. Fluid Mech.* **235**, 37–55.

MANKBADI, R. R. & LIU, J. T. C. 1981 A study on the interactions between large scale coherent structures and fine-grained turbulence in a round jet. *Phil. Trans. R. Soc. Lond.* A**28**, 541–602.

MATTINGLY, G. E. & CHANG, C. C. 1974 Unstable waves on an axisymmetric jet column. *J. Fluid Mech.* **65**, 541–560.

MICHALKE, A. 1971 Instabilitat eines compressiblen runden freistrahls unter berucksichtigung des einflusses der strahlgrenzschichtdicke. *Z. Flugwiss.* **19**, 319–328; also *NASA TM* 75190.

MONKEWITZ, P. A. & HUERRE, P. 1982 Influence of the velocity ratio on the spatial instability of mixing layers. *Phys. Fluids* **25**, 1137–1143.

PLASCHKO, P. 1979 Helical instabilities of slowly divergent jets. *J. Fluid Mech.* **92**, 209–215.

RAMAN, E. 1991 An experimental study of natural and forced modes in an axisymmetric jet. Ph.D. thesis, Case Western Reserve University.

REISENTHEL, P., XIONG, Y. & NAGIB, H. 1991 The preferred mode in an axisymmetric jet with and without enhanced feedback. *AIAA Paper* 91-0315.

RICE, E., RAMAN, E. & RESHOTKO, E. 1990 Measurement of naturally occurring modes in around jet. *Bull. Am. Phys. Soc.* **35**, 2322.

SANTOS, G. R. & HERBERT, TH. 1986 Combination resonance in boundary layers. *Bull. Am. Phys. Soc.* **31**, 1718.

SHAKIB, F. 1985 Evolution of interaction of instability modes in an axisymmetric jet. M.S. thesis, Illinois Institute of Technology, Chicago.

STRANGE, P. J. R. 1981 Spinning modes in orderly jet structure. Ph.D. thesis, University of Leeds, UK.

STRANGE, P. J. R. & CRIGHTON, D. G. 1981 Spinning modes on axisymmetric jets. *J. Fluid Mech.* **134**, 231–245.